JOURNAL OF PROPULSION AND POWER
Vol. 10, No. 3, May–June 1994

Dynamic Aeroelastic Stability of Vertical-Axis Wind Turbines Under Constant Wind Velocity

Fred Nitzsche*
DLR—Institute of Aeroelasticity, D-37073 Goettingen, Germany

The flutter problem associated with the blades of a class of vertical-axis wind turbines called Darrieus is studied in detail. The spinning blade is supposed to be initially curved in a particular shape characterized by a state of pure tension at the blade cross section. From this equilibrium position a three-dimensional linear perturbation pattern is superimposed to determine the dynamic aeroelastic stability of the blade in the presence of free wind speed by means of the Floquet-Lyapunov theory for periodic systems.

Nomenclature

A = area of the blade cross section
A_2, A_1, A_0 = apparent mass, aerodynamic damping, aerodynamic stiffness matrices, respectively
a = nondimensional location of the elastic axis measured from the midchord point in semichords (positive aft)
b = blade semichord
C = Coriolis matrix
$C(k)$ = Theodorsen's lift deficiency function
c_{d_0} = airfoil drag coefficient
E = Young's modulus
EA = axial stiffness
EI_{ii} = bending stiffness, $i = x$ (flatwise), y (chordwise)
G = shear modulus
GA = shear stiffness
GI_α = torsional stiffness
h = turbine's half height
K = stiffness matrix
k = reduced frequency
L_c, L_{nc} = circulatory and noncirculatory components of the lift
l = blade's total length
M = mass matrix
M_a = aerodynamic moment
M_i = component of the resultant moment at the cross section, $i = 1, 2, 3$
p = Laplace variable
Q_i = component of the resultant shear force at the cross section, $i = 1, 2$
q = state vector of the modal coordinates in the time domain
R = turbine's maximum radius (at "equator")
r = radial coordinate of the troposkien
r_α = radius of gyration of the cross section
s = spatial coordinate along the blade (from "north pole")
s_γ, c_γ = sin γ, cos γ (γ = any angular parameter)
t = time
u, v, w = local linear displacements of the elastic axis
V = local velocity of the wind relative to the blade cross section
V_∞ = undisturbed velocity of the wind relative to the ground
X = local tip speed ratio, $r\Omega/V$
X_∞ = turbine's tip speed ratio, $R\Omega/V_\infty$
$\boldsymbol{x}$ = state vector of the modal coordinates in the spatial domain
$x^{(n)}$ = nondimensional position of the blade's cross section neutral axis in semichords, Fig. 3a
x_α = nondimensional position of the blade's cross section center of mass in semichords, Fig. 3b
$\boldsymbol{y}^D$ = state vector of the displacement variables, $[u\chi_1 v\chi_2 w\alpha]^T$
1, 0 = unity matrix, null matrix
α = torsion of the blade cross section
ζ = vertical coordinate of the troposkien (Fig. 1)
Θ = azimuth angle, Ωt
$\kappa^{(0)}$ = local initial curvature of troposkien
Λ = fundamental transition matrix
λ = eigenvalues of the fundamental transition matrix
μ = mass ratio parameter, $\rho R^2/(\sigma A)_R$
ξ = structural damping factor
ρ = air density
σ = blade's material density
τ, $\tau^{(0)}$ = perturbation tension, initial tension of troposkien
φ = troposkien local angle, Eq. (A8)
Φ = modal matrix
χ_i = rotation of the blade cross section, $i = 1, 2$
Ω = turbine's spinning rate
ω = harmonic frequency

Subscripts
R = reference value
$,t$ = differentiation with respect to t $\partial/\partial t$
$,\theta$ = differentiation with respect to θ, $\partial/\partial\theta$

Superscripts
T = transpose of a matrix
$'$ = spatial derivative, $\partial/\partial s$
$*$ = characteristic value
$-$ = nondimensional quantity
$\tilde{}$ = diagonal matrix

Received July 10, 1993; revision received Sept. 3, 1993; accepted for publication Oct. 18, 1993.
*Scientist, DLR-WB-AE, Bunsenstr. 10. Member AIAA.

Introduction

TWO fundamental kinds of modern wind turbines have been investigated around the world: 1) the horizontal-axis (HAWT) and 2) the vertical-axis wind turbines (VAWT).

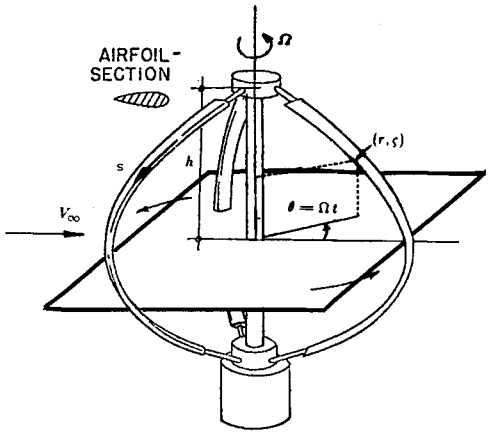

Fig. 1 Darrieus rotor.

The dynamics and aerodynamics of HAWT are better known, since the vast experience in propeller design of the aeronautical industry was employed to solve the important problems related to structural dynamics and aeroelasticity. However, VAWT, with their particular characteristics, have been challenging analysts.[1-9] Since modern VAWT are characterized by high spinning rates, for an observer sitting on the blade the flowfield is approximately parallel to the tangential motion of the airfoil. This observation led the former analyses to neglect the presence of the free wind speed V_∞ when performing flutter calculations. Although the free wind may be considered a second-order periodic perturbation on the airloads, it is ultimately responsible for the motion of the turbine and, therefore, is not disregarded in the present analysis. Moreover, accidents reported with some turbines have indicated that some improvement must be done on the existing theory so that the new generation of large and more economical machines may be considered fully reliable.

The troposkien shape[1,5,8] has sometimes been invoked in structural modeling of the blades of a special and particularly interesting VAWT; the Darrieus rotor (Fig. 1). When gravity is neglected, the troposkien is the plane curve described by a flexible rope rotating at a constant spinning rate. Its shape is known in closed analytical form.[8] Although a blade with such geometry is characterized as having no bending stress in the equilibrium position, tests have indicated that, under certain conditions, serious vibrations about the original position may occur. These vibrations involve in-plane (flatwise), out-of-plane (chordwise), and torsion of the structure. The intention of this article is to present an aeroelastic study of the troposkien-curved blade in the presence of free wind, observing the factors that may affect the dynamic stability of the structure. The mathematical model includes the most important parameters related to the VAWTs design, such as the center of mass (c.m.) and center of pressure (c.p.) offset from the elastic axis and the blade type of support. Effects like rotary inertia, shear deformation, extensibility, structural damping, and Coriolis are included as well.

Aeroelastic Equations of Motion

The general, second-order nonlinear aeroelastic equations of motion for a slender, nonuniform Darrieus blade were presented by Kaza and Kvaternik.[9] For physical understanding of the aeroelastic stability of a troposkien-curved blade, such degree of complexity seems unnecessary. However, it was decided that the number of degrees of freedom (DOF) of the blade cross section should be as large as six, containing the three linear displacements associated with the displacement of the reference axis from the troposkien equilibrium and the related three rotations of the cross section. Although it is possible to reduce the number of state variables by making reasonable assumptions such as blade inextensibility and negligible shear deformations, it seemed more effective to carry out the solution with the whole set of equations since important information may be inadvertently lost if premature simplifications are taken.

Small perturbations from the troposkien are assumed. The blade is considered a prestressed, untwisted, nonuniform rod on which a linear field of deformations is applied. The governing equations of motion for a three-dimensionally curved rod under a general initial stress configuration were obtained by different authors. Among them, Nair and Hagemier[10] use the state vector formulation to group these equations into a set of 12 first-order ordinary differential equations. The present work will proceed by taking these results, which were derived on the basis of the principle of virtual work. They satisfy the "hybrid formulation,"[11] where both the generalized force-related and the generalized displacement-related state variables are cast in a state vector form compatible with Reissner's principle of elasticity.

D'Alembert's principle and analytical dynamics methods are employed to obtain the dynamic loads that are experienced by the blade when it is rotating at a constant angular velocity. The c.m. offset, rotary inertia, Coriolis force, and gyroscopic moment effects are included. Gravity is neglected. The latter approximation is not only applicable for medium size, but also for some large VAWT on the basis of the lightness of the blade design.

Theodorsen's theory for thin airfoils oscillating in an incompressible flow is used to derive the external aerodynamic loads. The basic assumptions include: two-dimensional strip theory with the "simple sweep" idea (the airloads are unaffected by any component of the relative wind parallel to the local span), small angles of attack, no stall, and c.p. located at the quarter chord point. The fact that the optimum performance of Darrieus turbines occurs at high tip speed ratios contributes to assure small angles of attack and minimizes the possibility of stall. No attempt will be made to model the wake.

The linear aeroelastic equations of motion for a nonuniform blade originally curved in the troposkien shape were carefully derived in a former study.[12] The resultant set of equations takes the form (see Fig. 2)

$$Q_1' + \kappa^{(0)}\tau + f_1 = 0 \tag{1a}$$

$$Q_2' + f_2 = 0 \tag{1b}$$

$$\tau' - \kappa^{(0)}Q_1 + f_3 = 0 \tag{1c}$$

$$M_1' + \kappa^{(0)}M_3 - Q_2 - \tau^{(0)}\chi_1 + m_1 = 0 \tag{1d}$$

$$M_2' + Q_1 - \tau^{(0)}\chi_2 + m_2 = 0 \tag{1e}$$

$$M_3' - \kappa^{(0)}M_1 + m_3 = 0 \tag{1f}$$

$$u' + \kappa^{(0)}w - \chi_2 - [Q_1/(GA)_R] = 0 \tag{1g}$$

$$v' + \chi_1 - [Q_2/(GA)_R] = 0 \tag{1h}$$

$$w' - \kappa^{(0)}u - a_0[\tau/(EA)_R] + bx^{(n)}a_0[M_1/(EI_{xx})_R] = 0 \tag{1i}$$

$$\chi_1' + \kappa^{(0)}\alpha - a_0[M_1/(EI_{xx})_R] + bx^{(n)}a_0[\tau/(EI_{xx})_R] = 0 \tag{1j}$$

$$\chi_2' - [M_2/(EI_{yy})_R] = 0 \tag{1k}$$

$$\alpha' - \kappa^{(0)}\chi_1 - [M_3/(GI_\alpha)_R] = 0 \tag{1l}$$

In Eqs. (1i–1j)

$$a_0 = \left\{\frac{1}{1 - [bx^{(n)}]^2(EA)_R/(EI_{xx})_R}\right\} \tag{2}$$

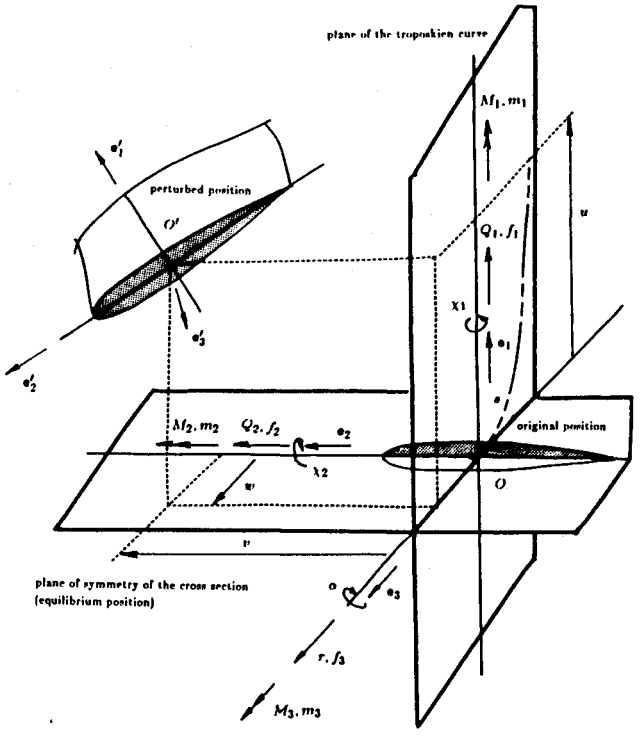

Fig. 2 Original and perturbed position of the blade cross section. Single arrows represent forces, double arrows moments. All perturbation quantities are measured in the reference frame defined by the undisturbed blade position (e_1, e_2, e_3).

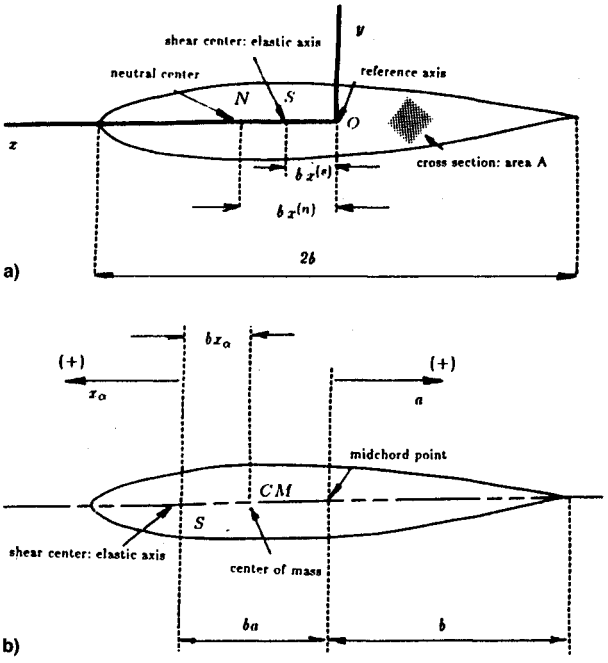

Fig. 3 Blade cross section definitions: a) structural and b) aeroelastic.

takes the unit value only if the neutral center coincides with the shear center. The cross section's definitions are depicted in Fig. 3a.

The total external load acting at the blade cross section is obtained by adding the dynamic and aerodynamic contributions

$$f_i = f_i^D + f_i^A \tag{3a}$$

$$m_i = m_i^D + m_i^A; \quad (i = 1, 2, 3) \tag{3b}$$

where f_i^D, m_i^D and f_i^A, m_i^A are respectively given by Eqs. (4a–4f) and Eqs. (16a–16d). In the Appendix, the parameters of Eqs. (1a–1l) associated with the troposkien geometry are sought:

$$-[f_1^D/(\sigma A)_R] = u_{,tt} + 2\Omega s_\varphi v_{,t} + \Omega^2 s_\varphi g - bx_\alpha \alpha_{,tt} - \underline{\Omega^2 r s_\varphi} \tag{4a}$$

$$-[f_2^D/(\sigma A)_R] = v_{,tt} + 2\Omega g_{,t} - \Omega^2 v + \underline{\Omega^2 b x_\alpha} \tag{4b}$$

$$-[f_3^D/(\sigma A)_R] = w_{,tt} - 2\Omega c_\varphi v_{,t} - \Omega^2 c_\varphi g + bx_\alpha \chi_{1,tt} + \underline{\Omega^2 r c_\varphi} \tag{4c}$$

$$-[m_1^D/(\sigma A)_R] = b^2(x_\alpha^2 + r_\alpha^2)\chi_{1,tt} + \Omega b^2 r_\alpha^2 s_\varphi \chi_{2,t} + (w_{,tt} - 2\Omega c_\varphi v_{,t} - \Omega^2 c_\varphi g) bx_\alpha + \underline{\Omega^2 b x_\alpha r c_\varphi} \tag{4d}$$

$$-[m_2^D/(\sigma A)_R] = -\Omega(s_\varphi \chi_{1,t} - c_\varphi \alpha_{,t} + \Omega\chi_2) b^2 x_\alpha^2 \tag{4e}$$

$$-[m_3^D/(\sigma A)_R] = b^2(x_\alpha^2 + r_\alpha^2)\alpha_{,tt} - \Omega b^2 r_\alpha^2 c_\varphi \chi_{2,t} - (u_{,tt} + 2\Omega s_\varphi v_{,t} + \Omega^2 s_\varphi g) bx_\alpha + \underline{\Omega^2 b x_\alpha r s_\varphi} \tag{4f}$$

where

$$g = c_\varphi(w + bx_\alpha \chi_1) - s_\varphi(u - bx_\alpha \alpha) \tag{5}$$

The terms underlined in Eqs. (4a–4f) are identified as steady-state components, related to the motion of the rigid blade. In the current stability analysis there is no interest in these components; thus, they are subtracted from the equations. The geometric aeroelastic parameters are defined in Fig. 3b.

The lift and pitching moments, per unit of span, due to both vertical translation and pitching of a two-dimensional airfoil, are defined in Eqs. (6a) and (6b)[13]:

$$L = \pi\rho b^2(u_{,tt} + V\alpha_{,t} - ba\alpha_{,tt}) + 2\pi\rho VbC(k)[u_{,t} + V\alpha + b(0.5 - a)\alpha_{,t}] \tag{6a}$$

$$M_\alpha = \pi\rho b^2[bau_{,tt} - Vb(0.5 - a)\alpha_{,t} - b^2(0.125 + a^2)\alpha_{,tt}] + 2\pi\rho Vb^2(a + 0.5)C(k)[u_{,t} + V\alpha + b(0.5 - a)\alpha_{,t}] \tag{6b}$$

In Eqs. (6a) and (6b) the first and second terms are known as the noncirculatory and circulatory components of the aerodynamic lift and moment about the elastic axis, respectively:

$$L = L_{nc}(t) + L_c(t, k) \tag{7a}$$

$$M_a = M_{a_{nc}}(t) + M_{a_c}(t, k) \tag{7b}$$

These components are shown in Fig. 4 according to their positive directions. The present analysis also includes the airfoil drag which acts at the c.p. and has a magnitude, per unit of blade span

$$D = \rho V^2 b c_{d_0} \tag{8}$$

When the airfoil moves in plunging motion alone, an induced angle of attack α_i is created:

$$\alpha_i = \tan^{-1}(u_{,t}/\sqrt{V^2 - \dot{u}^2}) \cong u_{,t}/V \tag{9}$$

The effective angle of attack is defined as the sum of the pitch angle and the induced angle of attack

$$\alpha_e = \alpha + u_{,t}/V \tag{10}$$

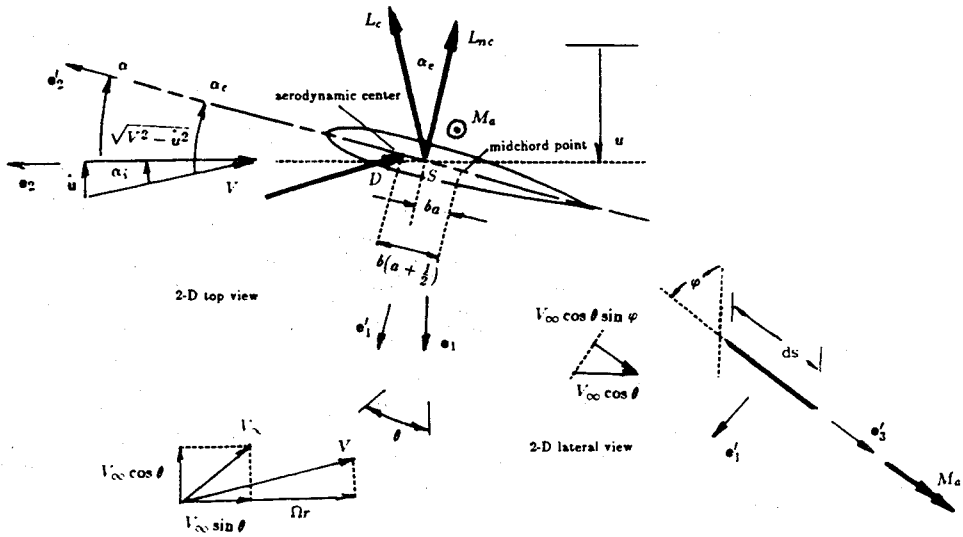

Fig. 4 Blade aerodynamics: top and lateral two-dimensional views of an elementary section along the blade.

According to the assumption of small angles, the nonzero vector components of the resultant aerodynamic force and aerodynamic moment are obtained from Fig. 4 using simple geometric considerations. In "disturbed" coordinates (e_1', e_2', e_3')

$$f_1^A = -L_c - L_{nc} - D\alpha_e = -L - D\alpha_e \tag{11a}$$

$$f_2^A = L_c\alpha_e - D \tag{11b}$$

$$m_2^A = M_a + b(a + 0.5)D\alpha_e \tag{11c}$$

These are transformed into the "undisturbed" coordinates (e_1, e_2, e_3)

$$\begin{bmatrix} f_1^A \\ f_2^A \\ f_3^A \end{bmatrix} = \begin{bmatrix} 1 & -\alpha & \chi_2 \\ \alpha & 1 & -\chi_1 \\ -\chi_2 & \chi_1 & 1 \end{bmatrix} \begin{bmatrix} f_1^A \\ f_2^A \\ 0 \end{bmatrix} \tag{12a}$$

$$\begin{bmatrix} m_1^A \\ m_2^A \\ m_3^A \end{bmatrix} = \begin{bmatrix} 1 & -\alpha & \chi_2 \\ \alpha & 1 & -\chi_1 \\ -\chi_2 & \chi_1 & 1 \end{bmatrix} \begin{bmatrix} 0 \\ 0 \\ m_3^A \end{bmatrix} \tag{12b}$$

after linearization yielding

$$f_1^A = -L - Du_{,t}/V \tag{13a}$$

$$f_2^A = -\underline{D} \tag{13b}$$

$$f_3^A = -D\chi_1 \tag{13c}$$

$$m_3^A = M_a + b(a + 0.5)D(\alpha + u_{,t}/V) \tag{13d}$$

The underlined term in Eq. (13b) is steady state and, thus, unimportant to the analysis. The derivation continues by seeking an approximation for the relative wind speed ratio V/V_∞, valid for the high tip speed ratios which characterize the optimum performance of Darrieus turbines [$X = \mathcal{O}(5)$]. Ashley,[14] using the "simple sweep" idea, calculated the aerodynamic effective components of the relative wind. Referring again to Fig. 4

$$V_1 = -V_\infty c_\theta c_\varphi \tag{14a}$$

$$V_2 = -\Omega r - V_\infty s_\theta \tag{14b}$$

From Eqs. (14a) and (14b), a linearization for the relative wind speed ratio is readily found

$$V/V_\infty = (\sqrt{V_1^2 + V_2^2}/V_\infty)$$

$$= X\sqrt{1 + 2s_\theta/X + \mathcal{O}(1/X^2)} \cong X + s_\theta \tag{15a}$$

by expanding the expression under the square root in powers of $1/X$. Likewise, a compatible linearization for the square of the relative speed ratio will be necessary:

$$(V/V_\infty)^2 \cong X^2(1 + 2s_\theta/X) = X^2 + 2Xs_\theta \tag{15b}$$

Substituting Eqs. (6a) and (6b) and (8) into Eqs. (13a–13d), and using Eqs. (15a) and (15b), the airloads are explicitly obtained in terms of the problem's state variables:

$$(f_1^A/\rho bV_\infty^2) = -\pi[(b/V_\infty^2)u_{,tt} + (X + s_\theta)(b/V_\infty)\alpha_{,t} - (b^2a/V_\infty^2)\alpha_{,tt}] - 2\pi C(k)q - c_{d_0}(X + s_\theta)(1/V_\infty)u_{,t} \tag{16a}$$

$$(f_3^A/\rho bV_\infty^2) = -c_{d_0}(X^2 + 2Xs_\theta)\chi_1 \tag{16b}$$

$$(m_3^A/\rho b^2V_\infty^2) = \pi[(ba/V_\infty)u_{,tt} - (X + s_\theta)(b/V_\infty) \times (0.5 - a)\alpha_{,t} - (b^2/V_\infty^2)(0.125 + a^2)\alpha_{,tt}] + 2\pi(a + 0.5)C(k)q + c_{d_0}(a + 0.5)[(X^2 + 2Xs_\theta)\alpha + (X + s_\theta)(1/V_\infty)u_{,t}] \tag{16c}$$

$$\frac{f_2^A}{\rho bV_\infty^2} = \frac{m_1^A}{\rho b^2V_\infty^2} = \frac{m_2^A}{\rho b^2V_\infty^2} = 0 \tag{16d}$$

where

$$q = (X + s_\theta)(1/V_\infty)u_{,t} + (X^2 + 2Xs_\theta)\alpha + (X + s_\theta)(b/V_\infty)(0.5 - a)\alpha_{,t} \tag{17}$$

General Flutter Analysis

The dynamic aeroelastic stability is studied by the classical modal superposition method. Two different situations are analyzed. The first is related to the forced motion of the Darrieus rotor by an external device such as a motor. The second is concerned with the actual work of the wind turbine when generating mechanical energy, assuming wind speed increasing from zero to characteristic values in the operating range.

The first situation is well suited for the root-locus method of tracing the roots of the so-called flutter determinant in the complex plane, since the airloads are easily converted in the frequency domain by taking their Laplace transform with respect to time. In the second case, the airloads generate differential equations with periodic coefficients and the

Floquet-Lyapunov theorem should be employed to determine the stability boundaries of the system.[15]

The modal superposition method is especially attractive when the natural free-vibration modes used to construct the aeroelastic modes are real-valued functions, once the well-known properties of the classical real eigenvalue problem remain valid. Although the free-vibration system has complex eigenvalues, generated by the Coriolis-related terms, it is still possible to work in the real domain by considering the Coriolis force as an additional external load acting at the blade cross section.

If the quasisteady approximation $[C(k \cong 1)]$ is taken, the flutter problem is described by the following matrix equation:

$$My''^{D} + Ky^{D} = -A_2 y''^{D} - (C + A_1)y'^{D} - A_0 y^{D} \quad (18)$$

The associated free-vibration eigenvalue problem, given by the left side of Eq. (18), is solved by an integrating-matrix scheme.[16] The m real eigenvectors of the "Coriolis-free" system can be organized in the modal matrix

$$\Phi = [{}^*y^{(1)} | {}^*y^{(2)} | \ldots | {}^*y^{(m)}] \quad (19)$$

A new set of dependent variables (modal coordinates) are defined by the linear transformation

$$y^{D} = \Phi x \quad (20)$$

where only x is time-dependent. Due to the harmonic time dependence of the modal coordinates, one has

$$x_{,\theta\theta} = -\Omega^2 x \quad (21)$$

$$(M\Phi\Omega^2 + K\Phi)x = 0 \quad (22)$$

Premultiplying Eq. (22) by Φ^T, one has

$$\Phi^T K \Phi = \mathbb{M}\Omega^2 \quad (23)$$

where

$$\mathbb{M} = \Phi^T M \Phi \quad (24)$$

is the matrix of generalized masses. Therefore, Eq. (18) reads in modal coordinates (nondimensional form):

$$(\mathbb{M} + \mu\bar{\mathbb{A}}_2)\bar{x}_{,\theta\theta} + (\mathbb{C} + \mu\bar{\mathbb{A}}_1)\bar{x}_{,\theta} + (\mathbb{M}\bar{\omega}^2 + \mu\bar{\mathbb{A}}_0)\bar{x} = 0 \quad (25)$$

where $\bar{\mathbb{A}}_2$, $\bar{\mathbb{C}}$, $\bar{\mathbb{A}}_1$, and $\bar{\mathbb{A}}_0$ are square matrices of dimension m, obtained by pre- and postmultiplication of the corresponding matrices in physical coordinates by $\bar{\Phi}^T$ and $\bar{\Phi}$, respectively. The aerodynamic matrices $\bar{\mathbb{A}}_0$ and $\bar{\mathbb{A}}_1$ may be written as the sum of two other matrices[12]:

$$\bar{\mathbb{A}}_1 = \bar{\mathbb{D}}_1 + (s_\theta/X_\infty)\bar{\mathbb{E}}_1 \quad (26)$$

$$\bar{\mathbb{A}}_0 = \bar{\mathbb{D}}_0 + (s_\theta/X_\infty)\bar{\mathbb{E}}_0 \quad (27)$$

From this point on, the bars denoting the nondimensional quantities will be dropped for the sake of the notation simplicity.

Zero Wind Speed Flutter Problem

If $1/X_\infty \to \infty$ (zero wind speed situation), it is straightforward to Laplace transform Eq. (25) with respect to time and obtain the flutter determinant in terms of simple matrix operations. Therefore, the characteristic values ${}^*p$ of the determinant are responsible for the aeroelastic stability:

$$|(\mathbb{M} + \mu\mathbb{A}_2){}^*p^2 + (\mathbb{C} + \mu\mathbb{A}_1){}^*p + \mathbb{M}\Omega^2 + \mu\mathbb{A}_0| = 0 \quad (28)$$

Muller's iterative complex root finder[17] is used to construct the root-loci of the first two aeroelastic modes as a function of the spinning rate. This result is presented in Fig. 5, as a plot of $\mathrm{Re}({}^*p)$ (the normalized modal damping) vs $\mathrm{Im}({}^*p) = \omega/\Omega$ (the normalized modal frequency). The case investigated corresponds to a Darrieus working at the sea-level air density, elastic axis at the quarterchord point, no structural damping, no c.m. offset, and pinned blades. The geometric and structural properties are listed in Table 1. It was observed that this turbine flutters at about 40 rpm, within its range of operation. To extend the stability boundaries of the same turbine to its entire operating range, it was necessary to introduce structural damping. The result obtained with a structural

Table 1 Darrieus rotor properties

l	24.1 m
h	8.5 m
Ω	29.8 – 52.5 rpm
$(\sigma A)_R$	10.22 kg/m
b	0.2665 m
r_α	0.10645
$(EI_{xx})_R$	357.56×10^4 N·m²
$(EI_{yy})_R$	9.0653×10^4 N·m²
$(GJ_\alpha)_R$	7.1972×10^4 N·m²
$(EA)_R$	231.83×10^6 N
$(GA)_R$	89.316×10^6 N

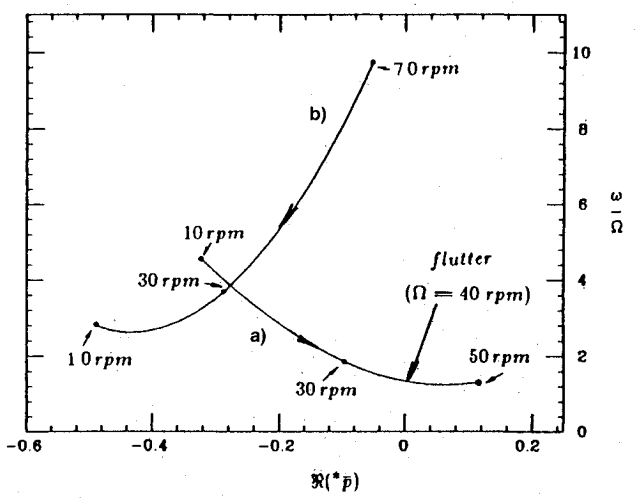

Fig. 5 Root loci vs Ω of the first two aeroelastic modes: a) flatwise bending-spanwise displacement and b) chordwise bending-torsion. μ = 6.05, ξ = 0, x_α = 0, a = −0.5. Pinned joints. V_∞ = 0.

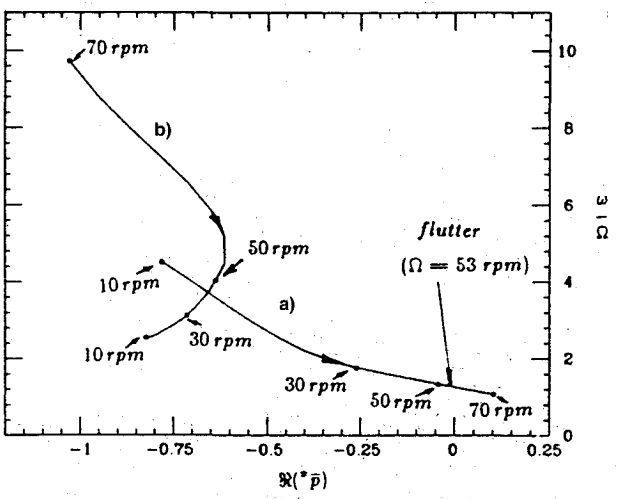

Fig. 6 Root loci vs Ω of the first two aeroelastic modes: a) flatwise bending-spanwise displacement and b) chordwise bending-torsion. μ = 6.05, ξ = 0.1, x_α = 0, a = −0.5. Pinned joints. V_∞ = 0.

damping of 10% is shown in Fig. 6. Structural damping can be readily introduced through a single term added to Eq. (27). The hypothesis involved is that the structural damping may be diagonalized by the modal matrix:

$$(\mathbb{M} + \mu\mathbb{A}_2)\boldsymbol{x}_{,\theta\theta} + (2\xi\mathbb{M}\omega + \mathbb{C} + \mu\mathbb{A}_1)\boldsymbol{x}_{,\theta} + (\mathbb{M}\omega^2 + \mu\mathbb{A}_0)\boldsymbol{x} = 0 \tag{29}$$

Another important conclusion from this preliminary study is that apparent mass has only a minor influence on the results. The stability boundaries are increased by an amount less than 2% if the matrix $\mathbb{A}_2$ is included in the mathematical model. This observation is also relevant for the next nonzero wind analysis.

Nonzero Wind Speed Flutter Problem

When a nonzero wind speed configuration is considered, the periodic terms in Eqs. (26) and (27) are present. Based on the above results, apparent mass is neglected, and Eq. (25) is premultiplied by the inverse of the generalized mass matrix, yielding

$$\boldsymbol{x}_{,\theta\theta} + \mathbb{H}_1\boldsymbol{x}_{,\theta} + \mathbb{H}_0\boldsymbol{x} = 0 \tag{30}$$

Here

$$\mathbb{H}_1 = \mathbb{M}^{-1}\{\mathbb{C} + \mu[\mathbb{D}_1 + (s_\theta/X_\infty)\mathbb{E}_1]\} \tag{31}$$

$$\mathbb{H}_0 = \omega^2 + \mu\mathbb{M}[\mathbb{D}_0 + (s_\theta/X_\infty)\mathbb{E}_0] \tag{32}$$

The period of revolution of the blade may be normalized to one if a new time scale is introduced ($\bar{\theta} = \theta/2\pi$). In state vector form, Eq. (30) reads

$$\boldsymbol{q}_{,\bar{\theta}} = \begin{bmatrix} \boldsymbol{x}_{,\bar{\theta}} \\ \boldsymbol{x} \end{bmatrix}_{,\bar{\theta}} = \begin{bmatrix} -\bar{\mathbb{H}}_1 & -\bar{\mathbb{H}}_0 \\ 1 & 0 \end{bmatrix} \boldsymbol{q} \tag{33}$$

where $\bar{\mathbb{H}}_1 = 2\pi\mathbb{H}_1$, and $\bar{\mathbb{H}}_0 = 4\pi^2\mathbb{H}_0$.

The nature of the eigenvalues of the transition matrix of the system over a single period will, according to the Floquet-Lyapunov theorem, determine the stability of the system. The same integrating-matrix scheme used to solve the free-vibration eigenvalue problem is employed to derive the transition matrix over the unitary period:

$$(\boldsymbol{q})_{\bar{\theta}=1} = \Lambda(\boldsymbol{q})_{\bar{\theta}=0} \tag{34}$$

The stability requires that for all eigenvalues of Λ

$$\mathrm{Re}(\lambda_i)^2 + \mathrm{Im}(\lambda_i)^2 < 1; \qquad (i = 1, 2, \ldots, 2m) \tag{35}$$

where

$$\mathrm{Re}(^*p_i) = \ln[\mathrm{Re}(\lambda_i)^2 + \mathrm{Im}(\lambda_i)^2]/2 \tag{36}$$

As in the previous section, two aeroelastic modes are studied. By varying X_∞, successive eigenvalues are extracted from Λ, and the stability is checked. Figure 7 depicts the modal damping coefficient calculated with Eq. (36) for the first two aeroelastic modes of a pinned blade spinning at 50 rpm, and the wind speed varying in such a way that the tip speed ratio lies within the operating range of the turbine. The free wind has a second-order effect on the flutter of the troposkien blade due to the order of magnitude of the tip speed ratios encountered in the real performance of the Darrieus. The cases investigated are the counterparts of the situations presented in Figs. 5 and 6. In the top figure ($\xi = 0$) an unstable branch (a) is observed, whereas in the bottom figure ($\xi = 0.1$) the unstable branch stabilizes itself. In both situations the higher the tip speed ratio, the worse the stability of branch (a) and

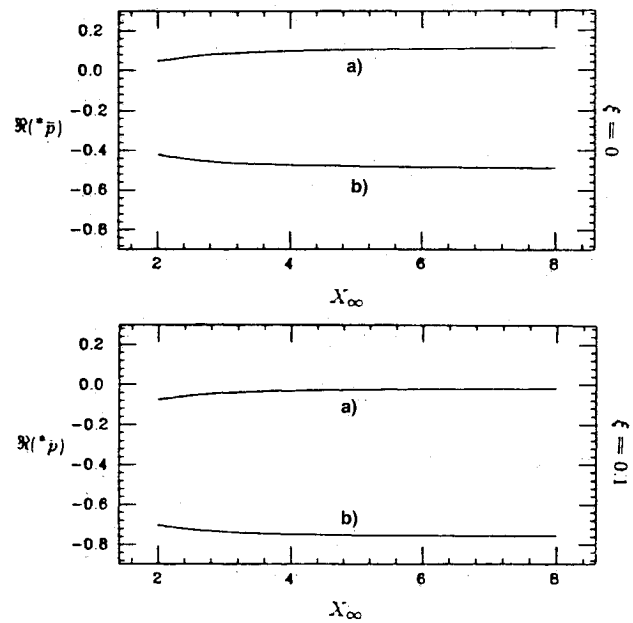

Fig. 7 Modal damping coefficient evolution with X_∞ of the first two aeroelastic modes: a) flatwise bending-spanwise displacement mode and b) chordwise bending-torsion mode. Top figure: $\xi = 0$; bottom figure: $\xi = 0.1$, $\mu = 6.05$, $x_\alpha = 0$, $a = -0.5$, $\Omega = 50$ rpm. Pinned joints.

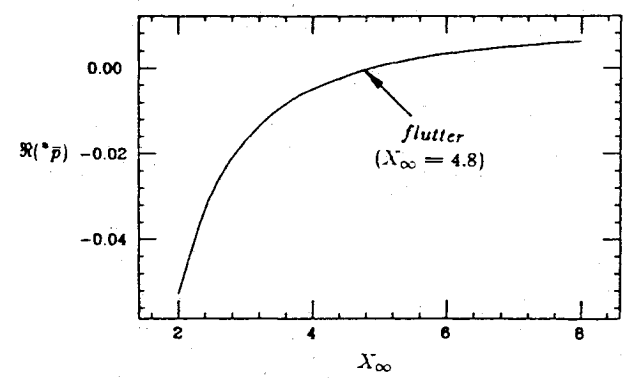

Fig. 8 Flatwise bending-spanwise displacement mode. Modal damping coefficient evolution with X_∞, $\mu = 6.05$, $\xi = 0.08$, $x_\alpha = 0$, $a = -0.5$, $\Omega = 50$ rpm. Pinned joints.

the better the stability of branch (b). Figure 8 depicts a particularly interesting situation where the flutter point is spotted at about $X_\infty = 4.8$ for $\xi = 0.08$.

Figure 9 presents a comparison between pinned and clamped blades. All structural and geometric properties remain the same except for the c.m. offset, which is now introduced (5% of the blade chord, the elastic axis lying behind the c.m.). When this case (top figure) is compared to its counterpart shown in Fig. 7, one concludes that the c.m. offset has little effect on the stability. However, the bottom figure shows that the most effective way of providing extra stability margins to Darrieus rotors is to restrain the blade's attachments. The flatwise bending-spanwise displacement mode becomes the most stable, exchanging its relative position with the chordwise bending-torsion mode. Although there is a slight destabilizing tendency in the latter branch as the tip speed increases, the stability boundary is never reached in the operating range of the turbine.

A convenient way to check some of the present flutter calculations is to compare the modal damping coefficients obtained by different methods: the zero wind case against the nonzero wind case, taking the limit of the latter as the airspeed decreases towards zero with the turbine still in operation ($X_\infty \to \infty$). Within the limits of accuracy of the theories applied, they should match [Eq. (36)]. Table 2 displays the result

Table 2 Re(*p)[a]

Mode	Laplace transform	Floquet-Lyapunov
1st	0.1165	0.1165
2nd	−0.4926	−0.4906

[a]Pinned blade at sea level, $\xi = 0$, $x_\alpha = 0$, $a = -0.5$, $\Omega = 50$ rpm, and $1/X_\infty = 0$.

Table 3 ω/Ω[a]

Mode	Complete problem	Modal superposition
1st	1.330	1.313
2nd	2.873	2.891

[a]Pinned blade at $\mu = 0$, $\xi = 0$, $x_\alpha = 0$, and $\Omega = 50$ rpm.

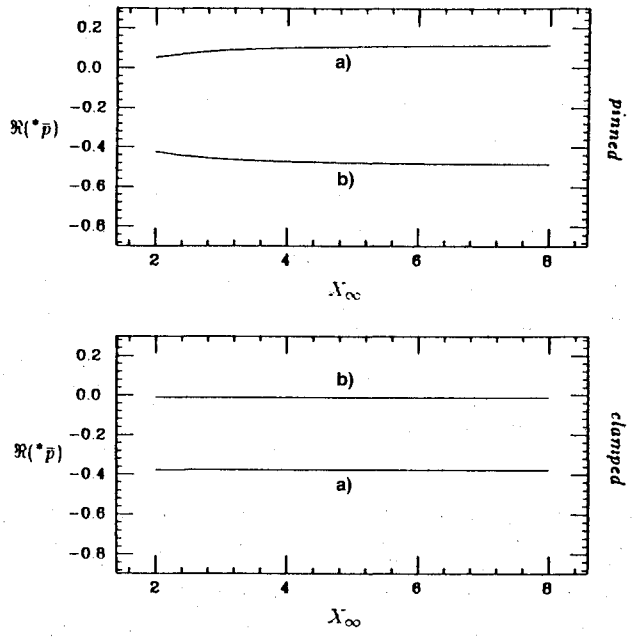

Fig. 9 Modal damping coefficient evolution with X_∞ of the first two aeroelastic modes: a) flatwise bending-spanwise displacement mode and b) chordwise bending-torsion mode. Top figure: pinned joints; bottom figure: clamped joints. $\mu = 6.05$, $\xi = 0$, $x_\alpha = -0.1$, $a = -0.5$, $\Omega = 50$ rpm.

of such a comparison for one particular case. The agreement is perfect for the first aeroelastic mode, and a relative error of only 0.004 is observed for the second mode.

Another question that will be investigated next is concerned with the number of free-vibration modes employed to construct the modal matrix and, consequently, the aeroelastic modes. This aspect of the problem is particularly important since the free-vibration modes used in the present analysis were not actual, but fictitious ones obtained by artificially dropping the Coriolis terms from the problem's original formulation. Table 3 answers this question by comparing the first two eigenvalues associated, the "complete" dynamics (including Coriolis effects) against the "Coriolis-free" results. The low errors observed guarantee the reliability of the present analysis.

Conclusions

The complete dynamic aeroelastic analysis of the Darrieus rotor was performed. Some important conclusions may be drawn from the mathematical model introduced:

1) Flutter may be an important source of failure of such VAWT. Situations were observed in which the blades became unstable within the operating range of the turbine. The free wind speed has a secondary influence in the results, but at least in one particular situation the turbine fluttered at a finite value of tip speed ratio.

2) Structural damping plays an important role in the stability analysis.

3) Nevertheless, the blade's boundary conditions ultimately determine the stability. The Coriolis effect plays a fundamental role in the system's dynamics, coupling together free mode shapes originally orthogonal at the null spinning rate (i.e. flatwise, chordwise, and torsion). It became clear that the designer should choose a more restrained blade support: clamped joints provided better safe margins as opposed to pinned joints. Actual design conditions must lie between the two extreme situations, but manufacturing solutions should increase the degree of attachment of the blade rather than decrease it.

The theory provides space for the inclusion of unsteadiness of the flow [$C(k) \neq 1$], but no numerical example was presented because it would require an extension of Theodorsen's lift deficiency function in terms of the azimuth angle for the case of the nonzero wind. Moreover, the quasisteady approximation is generally regarded as valid for the low reduced frequencies which characterize the operation of the Darrieus turbine.

Appendix: The Troposkien

Blackwell and Reis[8] coined the word "troposkien" to describe a geometric shape assumed by a perfect flexible cable of uniform density with its ends attached to two fixed points and turning at a constant angular velocity (from the Greek: tropo = turning and skien = rope). It is a well-defined shape and, as in the case of the catenary curve, its geometry is known in a closed mathematical form in terms of elliptical functions:

$$\zeta/h = 1 - [F(\phi, c)/F(\pi/2, c)] \tag{A1}$$

where

$$F(\phi, c) = \int_0^\phi d\varphi/\sqrt{1 - c^2 s_\varphi^2} \tag{A2}$$

$$c^2 = 1/[1 + (4/\Theta^2\beta^2)] \tag{A3}$$

and $\phi = \sin^{-1}(r/R)$. In Eq. (A3)

$$\Theta = \sqrt{1 - c^2}F(\pi/2, c) \tag{A4}$$

is a rotational parameter, and β is the ratio of the maximum horizontal displacement to the maximum vertical displacement of the cable, $\beta = R/h$. Thus, the process of numerically determining the troposkien shape is iterative. It is necessary to search the parameter c which satisfies a constraint equation:

$$l/2h = \frac{2}{1 - c^2}\frac{E(\pi/2, c)}{F(\pi/2, c)} - 1 \tag{A5}$$

where $F(\pi/2, c)$ and $E(\pi/2, c)$ are the complete elliptic integrals of the first and second kind with parameter c, respectively. Once the parameter is determined, it is possible to calculate the maximum tension in the cable, which occurs at the point of maximum horizontal displacement—the turbine's equator:

$$\tau_{\max} = (\sigma A)_R \Omega^2 h^2/\Theta^2 \tag{A6}$$

Some algebraic manipulations on the previous collection of results[12] lead to two other important relations: 1) the initial curvature

$$\bar{\kappa}^{(0)} = l\kappa^{(0)} = l/h\{\Theta^2\beta s_\phi/[1 + (\Theta^2\beta^2/2)c_\phi^2]^2 \tag{A7}$$

and 2) the local cable angle

$$\varphi = \sin^{-1}\{1/[1 + (\Theta^2\beta^2/2)c_\phi^2] \tag{A8}$$

defined by the normal to the cable at a certain location along the blade and the vertical axis (Fig. 4). An approximation for Eqs. (A7) and (A8) in terms of Chebyshev polynomials, useful for the discretization of the troposkien curve, may also be obtained.[12]

The initial tension can be decomposed in terms of the local cable angle and its vertical component:

$$\tau^{(0)} = \tau_v^{(0)}\sqrt{1 + (\tau_H^{(0)}/\tau_v^{(0)})^2} = \tau_v^{(0)}/s_\varphi \qquad \text{(A9)}$$

Because there is no gravity field, the vertical component of the tension remains constant along the blade. In particular, at the equator

$$\tau_v^{(0)} = \tau_{\max} \qquad \text{(A10)}$$

Hence

$$\tau^{(0)}/\tau_{\max} = 1/s_\varphi \qquad \text{(A11)}$$

Acknowledgment

I wish to express my gratitude to my Ph.D. advisor, Holt Ashley, for introducing me to the ever-exciting world of aeroelasticity and for his invaluable guidance throughout this research, held at Stanford University, Stanford, California, between 1980 and 1983. Today, though retired at age 70, he still inspires the work of most of his ex-students, as an ideal of professional excellence.

References

[1]Ham, N. D., "Aeroelastic Analysis of a Troposkien-Type Wind Turbine," Sandia Labs., SAND 77-0026, Albuquerque, NM, April 1977.

[2]Ottens, H. H., and Zwaan, R. J., "Investigations on the Aeroelastic Stability of Large Wind Turbines," National Aerospace Lab., NLR MP 78014-U, The Netherlands, April 1978.

[3]Lobitz, D. W., "Dynamic Analysis of Darrieus Vertical Axis Wind Turbine Rotors," Sandia Labs., SAND 80-2820, Albuquerque, NM, 1981.

[4]Popelka, D., "Aeroelastic Stability of a Darrieus Wind Turbine," Sandia Labs. Rept. SAND 82-0672, Albuquerque, NM, Feb. 1982.

[5]Meyer, E. E., "An Aeroelastic Analysis of the Darrieus Wind Turbine," Ph.D. Dissertation, Oregon State Univ., Corvallis, OR, 1982.

[6]Lobitz, D. W., "NASTRAN-Based Software for the Structural Dynamic Analysis of Vertical and Horizontal Axis Wind Turbines," Sandia Labs., SAND 84-0547, Albuquerque, NM, 1984.

[7]Rosen, A., and Abramovich, H., "Investigation of the Structural Behavior of the Blades of a Darrieus Wind Turbine," *Journal of Sound and Vibration*, Vol. 100, No. 4, 1985, pp. 493–509.

[8]Blackwell, B. F., and Reis, G. E., "Blade Shape for a Troposkien Type of Vertical-Axis Wind Turbine," Sandia Labs., SLA 74-0154, Albuquerque, NM, April 1974.

[9]Kaza, K. R. V., and Kvaternik, R. G., "Aeroelastic Equations of Motion of a Darrieus Vertical-Axis Wind-Turbine Blade," NASA TM-79295, Dec. 1979.

[10]Nair, S., and Hagemier, G., "Effect of Initial Stresses on the Small Deformations of a Composite Rod," *AIAA Journal*, Vol. 16, No. 3, 1978, pp. 212–217.

[11]Lehman, L. L., "Hybrid State Vector Methods for Structural Dynamic and Aeroelastic Boundary Value Problems," NASA CR-3591, Aug. 1982.

[12]Nitzsche, F., "Aeroelastic Analysis of a Darrieus Type Wind Turbine Blade with Troposkien Geometry," Ph.D. Dissertation, Stanford Univ., Stanford, CA, June 1983.

[13]Bisplinghoff, R. L., Ashley, H., and Halfman, R. L., *Aeroelasticity*, Addison-Wesley, Reading, MA, 1955, p. 272.

[14]Ashley, H., "Some Contributions to Aerodynamic Theory for Vertical-Axis Wind Turbines," *Journal of Energy*, Vol. 2, No. 2, 1978, pp. 113–119.

[15]Friedmann, P., Hammond, C. E., and Woo, T.-H., "Efficient Numerical Treatment of Periodic Systems with Application to Stability Problems," *International Journal for Numerical Methods in Engineering*, Vol. 11, No. 7, 1977, pp. 1117–1136.

[16]Nitzsche, F., "A Revised Version of the Transfer Matrix Method to Analyze One-Dimensional Structures," *Proceedings of the AIAA/ASME/ASCE/AHS 24th Structures, Structural Dynamics and Materials Conference* (Lake Tahoe, CA), Vol. 2, AIAA, Washington DC, May 1983, pp. 129–136.

[17]Conte, S. D., and De Boor, C., *Elementary Numerical Analysis, An Algorithmic Approach*, 3rd ed., McGraw-Hill, New York, 1980, pp. 120–127.